Meng *et al.*
EURASIP Journal on Advances in Signal Processing (2023) 2023:93
https://doi.org/10.1186/s13634-023-01057-4

EURASIP Journal on Advances in Signal Processing

RESEARCH

Open Access

Estimation of LFM signal parameters using RD compressed sampling and the DFRFT dictionary

Shuo Meng[1], Chen Meng[1*] and Cheng Wang[1]

*Correspondence: 2895104899@qq.com

[1] Shijiazhuang Campus, Army Engineering University of PLA, Shijiazhuang 050000, China

Abstract

In this paper, a method combining random demodulator (RD) and discrete fractional Fourier transform (DFRFT) dictionary is suggested to directly estimate the parameters of linear frequency modulation (LFM) signals from compressed sampling data. First, the RD system parameters are modified in accordance with the characteristics of the LFM signal to produce effective compressed sampling data. Next, a DFRFT dictionary is built using the fractional Fourier transform theory, and sparse representation coefficients are obtained by reconstructing the compressed sampling data using the recovery algorithm and DFRFT dictionary. The signal exhibits characteristics that make it pulse under the best fractional transform order, so the problem of signal parameter estimation can be reduced to searching for the location of the maximum value of sparse representation coefficients. The location is determined by a parameter optimization algorithm, and from there, the initial frequency and Chirp rate of the LFM signal can be estimated. Lastly, simulation and real data tests are performed to confirm that the suggested method can directly be utilized to estimate the parameter of LFM signals using compressed sampling data in addition to having high sparse representation ability for LFM signals.

Keywords: Compressed sampling, Random demodulator, Linear frequency modulation signal, Discrete fractional Fourier transform, Parameter estimation

1 Introduction

Due to their robust anti-interference ability, low likelihood of interception, huge bandwidth, and other advantages, linear frequency modulated (LFM) signals are widely used in complicated electromagnetic environments [1–3]. By scrutinizing intercepted radar signals from hostile sources, crucial intelligence can be garnered for electronic reconnaissance purposes. This intelligence can influence the adversary while safeguarding the security of our own information, playing a pivotal role in determining the outcome of a conflict [4, 5]. As a ubiquitous radar signal, the precise estimation of the initial frequency and chirp rate of LFM signals constitutes a significant research topic in radar signal analysis. However, existing studies on the direct estimation of LFM signal parameters are generally based on the Nyquist sampling theorem. While these studies achieve direct parameter estimation for LFM signals with lower bandwidths, research regarding parameter estimation for LFM signals with larger or even ultra-wide bandwidths remains insufficient. With the development of information technology and the complex and dynamic electromagnetic environment, the bandwidth of LFM signals is constantly increasing. Employing the conventional Nyquist theorem for sampling such a vast broadband signal would exert considerable strain on the A/D converter and generate an overwhelming volume of sampled data, posing challenges for subsequent signal handling and analysis [6–8].

With the development of compressed sensing theory, compressed sampling methods have become increasingly enriched, broadening the idea of solving the problem of large bandwidth signal acquisition [9, 10]. Among them, Non-Uniform Sampling (NUS) [11–13], Random Demodulator (RD) [14–17], and Modulated Broadband Converter (MWC) [18–20] systems are more mature. These sampling systems, when compared to Nyquist sampling, can sample broadband signals with a lower sampling rate and fewer sampling points, reducing the pressure of signal transmission and storage.

In Ref [11], Luo proposed a novel non-uniform interrupted sampling repeater jamming (NUISRJ) technique that effectively enhances the interference effect on phase-coded radar signals. In Ref [12], Liu investigated the parameter estimation challenges associated with Hammerstein-Wiener nonlinear systems utilizing non-uniform sampling. In Ref [13], Mirigaldi introduced the Non-Uniform Adaptive Angular Spectrum (NUADAS) method, specifically applicable to applications involving coherent beam combining and beam alignment. In Ref [14], Zhao presented a redesigned random demodulator (RD) capable of sampling generalized bandlimited signals. Furthermore, in Ref [18], Tropp proposed a parameter estimation method for frequency hopping (FH) signals based on multi-measurement vector sparse Bayesian learning (MSBL) within the context of modulation wideband converters (MWC).

However, the non-uniform triggering circuit design within the NUS structure requires a minimum sampling interval no less than the Nyquist frequency, thus not fundamentally eliminating the influence of the Nyquist theorem. On the other hand, the MWC system is used as a compression sampling system specifically designed for multi frequency narrowband signals and is not suitable for compression sampling of LFM signals.

Considering that the RD system employs a Fourier transform (FT) dictionary as the sparse representation dictionary, it is better suited for compressed sampling of frequency-domain sparse signals, particularly multi-tone signals. Compared to the MWC system, the RD system features a simpler and more implementable structure while avoiding the impact of Nyquist sampling frequency inherent in the NUS system's sampling process. Therefore, in this study, the RD system is selected as the compressed sampling system, achieving compressed sampling of LFM signals through the adjustment of RD system parameters and the construction of a novel sparse representation dictionary.

However, there is a dearth of research specifically devoted to the direct estimation of signal characteristics using compressed sample data, as the focus of compression sampling technology primarily lies in addressing the challenges of signal compression sampling and signal recovery [21–23]. It was not until 2010 that Davenport et al. laid the theoretical foundation for studying parameter estimation based on compressed samples [24], demonstrating the feasibility of directly estimating signal parameters from compressed sample data. In some instances, these techniques do not necessitate the reconstruction of the original signal; instead, they estimate the signal parameters by establishing a relationship between the parameter of interest and the coefficients of sparse representation derived from the compressed samples. Frequently, the construction of a sparse representation dictionary for signals becomes imperative in order to extract the coefficients that capture the sparsity properties of the signals.

In the early stages, the design of sparse dictionaries based on orthogonal transformations was mainly based on orthogonal FT dictionaries [25]. Due to the fact that FT dictionaries can only achieve sparse representation of one-dimensional signals, Shaik [26] proposed a combined FT dictionary for the analysis of dynamic nuclear magnetic resonance images. In Ref [27], Yu proposed a wavelet transform (WT) dictionary that can be used for sparse representation of two-dimensional image signals, while Wu [28] proposed a discrete cosine transform (DCT) dictionary that can be applied to studying the influence of fabric density on the representation of the fabric texture and detecting fabric flames. Due to their simplicity, these dictionaries have long been widely used. However, they are typically limited to representing low-dimensional signals, making it challenging to represent complex, high-dimensional signals. The limited representational capacity has restricted the development of these dictionaries. Broadband LFM signals, as complex nonlinear signals, cannot achieve ideal sparse representation using the sparse representation dictionary mentioned above. For broadband LFM signals, it comes as evidence that these dictionaries struggle to achieve desirable results [29, 30].

Therefore, it is necessary to explore new dictionaries or improve the structure of existing dictionaries to achieve sparse representation for LFM signals. Currently, sparse representations based on redundant dictionaries have gained widespread usage due to their versatility. Among them, the waveform matching dictionary proposed by Mirigaldi [13] is one form of redundant dictionary that requires prior information for its construction. However, obtaining prior information for LFM signals in complex electronic reconnaissance environments is not easily attainable.

The fractional Fourier transform (FRFT) is a time–frequency analysis method that can achieve time–frequency analysis of high-dimensional signals, avoiding the problems in the dictionaries mentioned above. In Ref [31], FRFT was used to analyze hyperspectral image signals, and some researchers have directly employed the FRFT method to estimate some narrowband LFM signal characteristics. These studies, however, continue to rely on the Nyquist sampling theory. When applied to the parameter estimation of LFM signals with hub broadband or even ultra-wideband bandwidth, the issue of creating mass volumes of data during the signal acquisition process cannot be avoided.

Inspired by the construction of sparse dictionaries, some researchers have combined the theory of FRFT with compressed sensing by constructing FRFT dictionaries. Against this backdrop, this paper introduces a method for parameter estimation of LFM signals based on the integration of Random Demodulator compressed sampling and a discrete fractional Fourier transform (DFRFT) dictionary.

The main work of the paper can be divided into two parts: firstly, the application of the RD compressive sampling system to compressively sample linear frequency modulation (LFM) signals; secondly, the parameter estimation of LFM signals under compressive sampling conditions using a DFRFT dictionary.

The innovative work of this paper can be summarized as follows: Addressing the problem of parameter estimation for LFM signals under RD compressive sampling conditions, this paper proposes a novel approach based on a DFRFT dictionary. This method demonstrates wide applicability and does not rely on prior information. Firstly, by leveraging the theory of fractional Fourier transform, the paper constructs the DFRFT dictionaries at different transform orders, which can be used for the sparse representation of LFM signals. Secondly, based on the characteristic impulse response of LFM signals in the optimal transform order, the relationship between LFM signal parameters and fractional order variables is derived, thereby transforming the parameter estimation problem into an optimization problem for the peak values of sparse representation coefficients. Then, the quantum particle swarm optimization (QPSO) algorithm is employed as the optimization tool to search for the peak values of the sparse coefficients. By utilizing the formulaic relationship between unknown parameters and peak values, the estimates for the initial frequency and frequency slope of the LFM signal are obtained. Finally, the effectiveness of the proposed method is validated through simulation experiments, and comparative analyses with other methods are conducted in Sect. 6.

This paper's remaining sections are organized as follows: The methodologies employed in the suggested work are presented in Sect. 2. The algorithmic performance evaluation is conducted in Sect. 3. The parameter estimation of simulated signals is conducted in Sect. 4. The measured signal analysis is conducted in Sect. 5. The work is concluded in Sect. 6, which also gives the approach's prospective future use.

2 Fundamental theory

2.1 FRFT

FRFT is the extension of FT. Assuming that the signal is $x(t)$, the FRFT of $x(t)$ can be expressed in the following linear integral form:

$$X_p(u) = \left\{F^p[x(t)]\right\}(u) = \int_{-\infty}^{+\infty} x(t) K_p(t,u) \mathrm{d}t \tag{1}$$

where $F^p[\cdot]$ is the FRFT operator, p indicates the transformation order; $K(\alpha, u, t)$ is a kernel function.

The kernel functional equation varies with rotation angle, as seen below:

$$K(\alpha,u,t) = \begin{cases} \sqrt{\frac{(1-j\cot\alpha)}{2\pi}} \exp\left[j\left(\frac{t^2+u^2}{2}\right)\cot\alpha - 2jtu\csc\alpha\right], & \alpha \neq n\pi \\ \delta(t-u), & \alpha = 2n\pi \\ \delta(t+u), & \alpha = (2n+1)\pi \end{cases} \tag{2}$$

where $n \in$ Z, Z denotes the integer field; δ is a Kronecker function; α denotes the rotation angle of FT, t is the integration variable, and u denotes the parameter variable of the fractional domain. The link between α and transformation order p can be written as: $\alpha = p\pi/2$, implying that the period of transformation order p is 4. According to the FRFT characteristics, when just examining the amplitude of the signal FRFT in the fractional order domain, the range of p can be further restricted to [0, 2), because the amplitude of the signal FRFT is the same whether p is taken in the interval [0, 2) or [2, 4). The time frequency plane rotation diagram of FRFT is shown in Fig. 1.

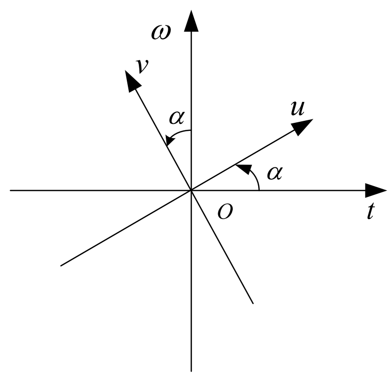

Fig. 1 Schematic diagram of time–frequency plane rotation

The plane created by (t, ω) in Fig. 1 is the time–frequency plane, where t is the time variable and ω is the frequency. The fractional-domain plane (u, v) is generated by rotating the original plane around the origin by an arbitrary angle of α, where u is a fractional-domain variable and v is a fractional-domain frequency. When α and p are both zero, and the FRFT of the signal $x(t)$ remains $x(t)$; when $\alpha = \pi/2$ and $p = 0$, the FRFT of the signal becomes the FT of the signal. When rotation angle α is varied, the transformation is fractional, which is also a generalized version of Fourier transform.

2.2 FRFT of LFM signal

The interdependent correlation between the initial frequency and chirp rate of the LFM signal and the fractional variable u and transform order p can be deduced when using the FRFT to analyze the LFM signal. Define the multi-component LFM signal as $x(t)$, which can be expressed as follows:

$$x(t) = \sum_{i=1}^{K} A_i \exp\left[j2\pi\left(f_i t + \frac{1}{2}k_i t^2\right)\right] \tag{3}$$

where K is the number of LFM signal components, A_i,f_i, k_i are amplitude, initial frequency, and Chirp rate of the ith component of the LFM signal, respectively.

The FRFT of the single component LFM signal is written as below:

$$X_p(u) = A\sqrt{\frac{1 - j\cot\alpha}{2\pi}} \int_{-\infty}^{+\infty} \exp\left[j\left(\frac{u^2 + t^2}{2}\right)\cot\alpha - jut\csc\alpha + j\pi\left(kt^2 + f_c t\right)\right]\mathrm{d}t \tag{4}$$

When $\alpha = \mathrm{arccot}(-k)$, Eq. (4) can be simplified as:

$$\begin{aligned} X_p(u) &= A\sqrt{\frac{1 - j\cot\alpha}{2\pi}} \int_{-\infty}^{+\infty} \exp\left[j\left(\frac{\mathrm{u}^2 + \mathrm{t}^2}{2}\right)\cot\alpha - jut\csc\alpha + j\pi\left(\cot\alpha t^2 + f_c t\right)\right]\mathrm{d}t \\ &= A\sqrt{1 - j\cot\alpha}\exp\left(j\pi u^2\cot\alpha\right)\int_{-\infty}^{+\infty} \exp(j(f_c t - 2tu\csc\alpha))\mathrm{d}t \end{aligned} \tag{5}$$

The integral term of Eq. (5) can then be simplified using the pulse function, yielding the following results:

$$X_p(u) = A\sqrt{1 - j\cot\alpha}\exp(j\pi u^2\cot\alpha) \times \delta[2\pi(u\csc\alpha - f_c)] \tag{6}$$

Equation (6) can be viewed as a pulse function of u because δ is a Kronecker function. When $\alpha = \operatorname{arccot}(-k)$, the single component LFM signal appears as a pulse in the fractional order domain.

Because the parameter information for the intercepted LFM signal is unknown in the real electronic reconnaissance process, the best transformation order p_{opt} corresponding to the rotation angle cannot be established directly. However, according to $\alpha = \operatorname{arccot}(-k) = p\pi/2$ and the FRFT of the LFM signal Eq. (4), the relationship between the chirp rate and the initial frequency of the LFM signal, as well as the best transformation order and the FRFT variable, is as follows:

$$\begin{cases} k = -\cot\alpha_{\text{opt}} = -\cot\left(\frac{p_{\text{opt}}\pi}{2}\right) \\ f_c = u_{opt}\csc(\alpha_{\text{opt}}) = u_{opt}\csc\left(\frac{p_{\text{opt}}\pi}{2}\right) \end{cases} \tag{7}$$

Therefore, the parameter estimation problem of LFM signal's chirp rate and initial frequency can be converted into the estimation of optimal order p_{opt} and FRFT variable u_{opt}.

However, in real-world scenarios, it is also required to take the pulse of the signal length and sampling frequency into account in order to determine the best order and the estimated value $(\widehat{p}_{\text{opt}}, \widehat{u}_{\text{opt}})$ of the FRFT variable. The following equation must be used to determine the real parameter estimates [13]:

$$\begin{cases} \widehat{k} = -\frac{f_s^2}{(N-1)}\cot\widehat{\alpha}_{\text{opt}} = -\frac{f_s^2}{(N-1)}\cot\left(\frac{\widehat{p}_{\text{opt}}\pi}{2}\right) \\ \widehat{f_c} = u_{\text{opt}}\sqrt{\frac{f_s^2}{(N-1)}}\csc(\widehat{\alpha}_{\text{opt}}) = \widehat{u}_{\text{opt}}\sqrt{\frac{f_s^2}{(N-1)}}\csc\left(\frac{\widehat{p}_{\text{opt}}\pi}{2}\right) \end{cases} \tag{8}$$

where N is the signal length and f_s are the sampling frequency.

Upon completion of the correlation analysis for parameter estimation of a single-component LFM signal, the application of FRFT can be extended to multi-component LFM signals. In fact, the FRFT analysis of multi-component LFM signals can be regarded as the superposition of multiple single-component LFM signals. Thus, Eq. (6) can be generalized to describe the FRFT of multi-component LFM signals.

$$X(v) = \sum_{i=1}^{K} X_{p,i}(u_i) \tag{9}$$

where $X(v)$ is the FRFT of K-component LFM signal.

Similarly, the estimation of frequency slope and initial frequency for multi-component LFM signals can be considered an extension of the parameter estimation process for single-component LFM signals. By generalizing Eq. (8), the estimation results for the initial frequency and frequency slope of the i-th component of the LFM signal can be obtained.

$$\begin{cases} \widehat{k}_i = -\frac{f_s^2}{(N-1)}\cot\widehat{\alpha}_{\text{opt},i} = -\frac{f_s^2}{(N-1)}\cot\left(\frac{\widehat{p}_{\text{opt},i}\pi}{2}\right) \\ \widehat{f}_{c,i} = u_{\text{opt},i}\sqrt{\frac{f_s^2}{(N-1)}}\csc(\widehat{\alpha}_{\text{opt},i}) = \widehat{u}_{\text{opt}}\sqrt{\frac{f_s^2}{(N-1)}}\csc\left(\frac{\widehat{p}_{\text{opt},i}\pi}{2}\right) \end{cases} \tag{10}$$

where $p_{\mathrm{opt},i}$,$u_{\mathrm{opt},i}$ and $\alpha_{\mathrm{opt},i}$ correspond to the optimal transform order, fractional order variable and rotation angle of the i-th component signal, respectively.

2.3 DFRFT

The closed-form discrete fractional Fourier transform (CF-DFRFT) approach suggested in Ref [32] is used to create the DFRFT dictionary. The theoretical analysis of this straightforward, reversible procedure is as follows.

Firstly, the input $x(t)$ and output $X_p(u)$ in Eq. (1) are discretized with sampling intervals of Δt and Δu, respectively. The discretized Eq. (1) can be expressed as follows:

$$\begin{aligned} X_p(m) &= \sum_{n=-N}^{N} K_p(m,n)x(n) \\ &= \sqrt{\frac{1-j\cot\alpha}{2\pi}}\Delta t \exp\left(\frac{j}{2}\cot\alpha m^2\Delta u^2\right)\cdot \\ &\quad \sum_{n=-N}^{N}\exp(-j\csc\alpha nm\Delta u\Delta t)\cdot\exp\left(\frac{j}{2}\cot\alpha n^2\Delta t^2\right)\cdot x(n) \end{aligned} \tag{11}$$

where m and n are integers, and $m\in[-M,M]$,$n\in[-N,N]$.

For DFRFT, the reversibility must satisfy both of the following conditions:

$$\begin{cases} M\geq N \\ \Delta u\cdot\Delta t = 2\pi|\sin\alpha|/(2M+1) \end{cases} \tag{12}$$

When the above conditions are met, the discrete fractional Fourier reversible transformation is:

$$x(n) = \sum_{m=-M}^{M}\sum_{k=-N}^{N} K_p^H(m,n)K_p(m,k)\cdot x(k) \tag{13}$$

where $K_p^H(m,k)$ is conjugate transpose of $K_p(m,k)$.

When $\sin\alpha\neq 0$, substitute Eq. (12) into $K_p(m,k)$:

$$\begin{aligned} K_p(m,n) = &\sqrt{\frac{|\sin\alpha|-j\mathrm{sgn}(\sin\alpha)\cos\alpha}{2M+1}} \\ &\exp\left(\frac{j}{2}\cot\alpha m^2\Delta u^2\right)\cdot\sum_{n=-N}^{N}\exp\left(-j\frac{sgn(\sin\alpha)\cdot 2\pi nm}{2M+1}\right)\cdot \\ &\exp\left(\frac{j}{2}\cot\alpha n^2\Delta t^2\right) \end{aligned} \tag{14}$$

Since $K_p(m,n)$ is reversible, set $M=N$, the DFRFT dictionary is:

$$\boldsymbol{\Psi}_p = K_{-p} = K_p^H = \left[K_p(m,n)\right]^H, m,n\in[-N,N] \tag{15}$$

2.4 LFM signal parameter estimation based on compressed sampling

The following theoretical understanding is required, in accordance with compressed sensing theory, in order to estimate LFM signal parameters utilizing compressed sampling data that is output by the RD system.

(1) *Sparse representation*. The sparse representation of signals is a necessary condition of the compression sensing theory, so a sparse dictionary is constructed to achieve the sparse representation of LFM signals. The sparse expression formula for signal $\boldsymbol{x}$ is as follows:

$$\mathbf{x} = \Psi\mathbf{r} \tag{16}$$

where $\boldsymbol{\Psi}$ is a sparse dictionary and $\mathbf{r}$ is the coefficient vector of sparse representation.

(2) *Compression observation*. The compressed sampling data is obtained by measuring the signal with the observation matrix, and the equation is:

$$\mathbf{y} = \Phi\mathbf{x} = \Phi\Psi\mathbf{r} \tag{17}$$

where $\mathbf{y}$ is measured value of compression observation and $\boldsymbol{\Phi}$ is the measurement matrix.

In this paper, LFM signals are compressed and sampled using the RD system. Figure 2 depicts the RD system's organizational structure. In the RD system, the observation matrix $\boldsymbol{\Phi}$ is actually created by multiplying the discrete matrix of the low-pass filter pulse response function $h(t)$ and the random sequence $p(t)$, which may be written as the following equation:

$$\boldsymbol{\Phi} = \mathbf{HP} \tag{18}$$

where $\mathbf{P}$ is the diagonal matrix of size $W \times W$ obtained by discretization of random sequence $p(t)$, W is Nyquist sampling frequency, the elements on the diagonal are $\varepsilon_n(\pm 1)$, the remaining elements are zeros. The size of $\mathbf{H}$ matrix is $R \times W$, and the i-th row of $\mathbf{H}$ is the reverse order of $i \times C$ elements before filter impulse response $h(n)$. When the number of elements of $h(n)$ is less than $i \times C$, zero is added to the end of $h(n)$ before the reverse order, and then the reverse order, and $C = W/R$. After the input signal $x(t)$ is compressed and sampled by the RD system, the compressed sampling data $y[m]$ is obtained.

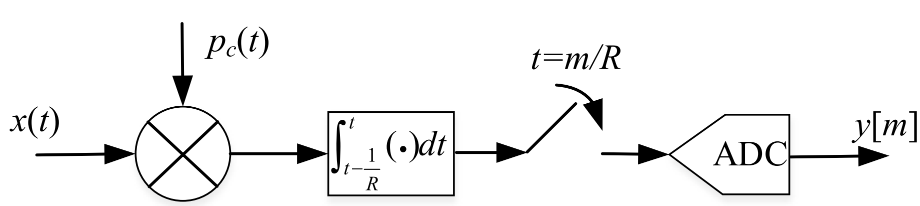

Fig. 2 RD

(3) *Parameter estimation*. Using the recovery algorithm to reconstruct the measured value $\mathbf{y}$, the sparse coefficient $\mathbf{r}$ of the signal can be obtained. When the DFRFT dictionary $\boldsymbol{\Psi}_p$ is selected as the sparse dictionary, the corresponding sparse representation coefficient $\mathbf{r}_{\mathrm{p}}$ is obtained. The $|\mathbf{r}_{\mathrm{p}}|$ physical meaning is the amplitude corresponding to the p-order fraction of the LFM signal. Therefore, the value interval of the transformation order p can be set as [0, 2). According to Eq. (15), the construction of dictionary $\boldsymbol{\Psi}_p$ is related to the value of transformation order p. Therefore, the transformation order p is traversed in the interval [0, 2), and $\boldsymbol{\Psi}_p$ under different orders is constructed to obtain the DFRFT dictionary library $\boldsymbol{\Psi}_{FR}$. Combined with the recovery algorithm, $\mathbf{y}$ is reconstructed, and $\mathbf{r}_{\mathrm{FR}}$ is calculated, $|\mathbf{r}_{\mathrm{FR}}(p,u)|$ are two-dimensional distributions about (p,u). According to Eq. (8), LFM signals only have the best sparsity in the dictionary constructed by the optimal order p, that is, the $|\mathbf{r}_{\mathrm{FR}}(p_{\mathrm{opt}},u_{\mathrm{opt}})|$ shows obvious pulse characteristics. Therefore, the estimation of the optimal transformation order p_{opt} and fractional order variable u_{opt} is converted into the search for the location of $|\mathbf{r}_{\mathrm{FR}}(p,u)|$ peak value. The mathematical model is as follows:

$$\begin{cases} \{\widehat{p}_{\mathrm{opt}},\widehat{u}_{\mathrm{opt}}\}=\arg\max\limits_{p,u}|\mathbf{r}_{\mathrm{FR}}(p,u)| \\ p\in[0,2) \\ u\in\forall \end{cases} \tag{19}$$

The $(\widehat{p}_{\mathrm{opt}}, \widehat{u}_{\mathrm{opt}})$ can be obtained by solving the above model, then the estimated Chirp rate and initial frequency can be calculated combined with Eq. (8).

The above process of parameter estimation based on compressed sampling can be summarized as follows:

Step 1 The RD system is used to compress and sample the signals, and output is $y[m]$.
Step 2 To calculate the coefficient vector $\mathbf{r}_{\mathrm{FR}}$, the reconstruction algorithm and DFRFT dictionary are used to reconstruct the compressed sampling data.
Step 3 Search for the peak position of $|\mathbf{r}_{\mathrm{FR}}(p,u)|$ using the parameter optimization algorithm, and the $(\widehat{p}_{\mathrm{opt}},\widehat{u}_{\mathrm{opt}})$ is obtained.
Step 4 Determine the LFM signal parameters $(\widehat{f_c}, \widehat{k})$ using $(\widehat{p}_{\mathrm{opt}},\widehat{u}_{\mathrm{opt}})$ and Eq. (8).

2.5 QPSO

For the peak search problem of two-dimensional distribution, the commonly used algorithms include direct search, two-dimensional search algorithms, etc., but these algorithms are computationally heavy and time-consuming. The particle swarm optimization (PSO) algorithm can improve the search efficiency based on the above methods, but it is easy to fall into local optimization. Therefore, based on the theory of quantum mechanics, Xu et al. [33] reduced the complexity of the algorithm, improved the global search ability of the algorithm, and solved the problem of local optimization by quantifying the particle iterative update process in the PSO algorithm. Therefore, the QPSO algorithm is used to search for the peak value of $|\mathbf{r}_{\mathrm{FR}}(p,u)|$ to ensure the accuracy and timeliness of parameter estimation. Based on the QPSO algorithm, the peak search process of $|\mathbf{r}_{\mathrm{FR}}(p,u)|$ using QPSO can be concluded as follows:

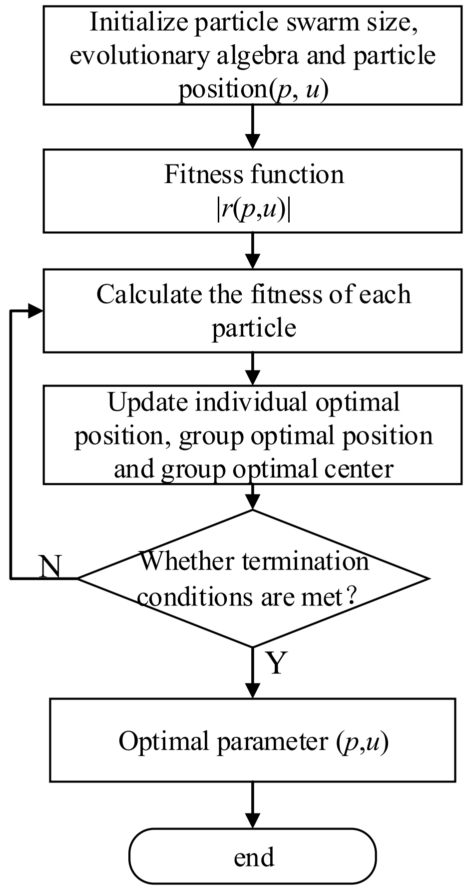

Fig. 3 Parameter optimization process based on QPSO

Step 1 Initialize the particle position of the population and configure parameters such as particle swarm size, iteration step size, and termination conditions;

Step 2 Initialize the current position of each particle, calculate the fitness of each particle with equation (19) as the fitness function, and initialize the position of the particle with the largest fitness;

Step 3 Update the particle position based on QPSO theory;

Step 4 Calculate the fitness of each particle and update the individual optimal position, group optimal position, and group optimal based on the best fitness value;

Step 5 Whether the termination condition is valid. If it is, stop the calculation and output the results; otherwise, return to step (3).

The above parameter optimization process can be summarized as shown in Fig. 3.

3 Algorithmic performance evaluation

3.1 Simulation signal

The simulation experiment environment of this manuscript is a Windows 10 64-bit operating system and Matlab R2018b software platform. The computer processor used in the simulation is an Intel Core i7-10875H, whose main frequency is 2.30 GHz, and the memory is 16.0 GB. Single-component and multi-component LFM signals are

Table 1 Parameters of simulation signal

Signal	K	A_i	f_i (MHz)	k (MHz/us)	T (us)
Signal 1	1	1	250	− 300	1
Signal 2	4	1	[100 200 300 400]	− 300	1

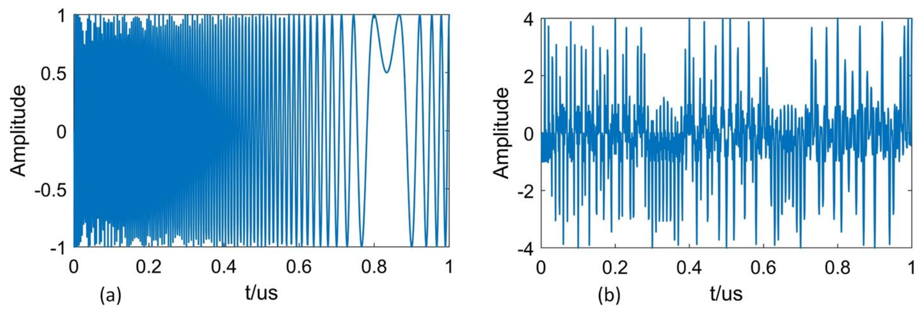

Fig. 4 Simulation signal. **a** Signal 1; **b** Signal 2

generated by Eq. (3). The signal parameter settings are shown in Table 1, the parameter meanings are shown in Eq. (3), and the signal time domain diagram is shown in Fig. 4.

3.2 Sparse representation analysis

The sparse representation of signals is the precondition for compressed sampling, which needs to be implemented by constructing a sparse dictionary. In order to highlight the sparse representation effect and noise resistance of the DFRFT dictionary, comparative experiments with different methods are designed, including:

Method (1): Fourier Transform (FT) dictionary.
Method (2): Wavelet Transform (WT) dictionary.
Method (3): Waveform Matching (WM) dictionary.
Method (4): DFRFT dictionary.

Method (1) was constructed with reference to [26], method (2) was constructed with reference to [27], and in method (3), the intervals [0 MHz, 500 MHz] and [− 500 MHz/us, 0 MHz/us] to which parameters f and k belong are divided into 50 parts, respectively, to obtain a waveform matching dictionary library with the size of 50×50. Method (4) constructs the sparse representation dictionary with the optimal transformation order. The sparse representation results and the descending coefficient arrangement of simulation signal 1 under different dictionaries are shown in Fig. 5, and the results of simulation signal 2 are shown in Fig. 6.

In Figs. 5 and 6, the results obtained by method (1) show poor sparsity, the attenuation speed of coefficients sorted by amplitude is slow, and the compressibility effect of the signal under this dictionary is poor; The fuzzy phenomenon occurs in the results obtained by using method (2) because the resolution ability of the WT dictionary is poor in the low-frequency part. Compared with method (1), the attenuation speed of

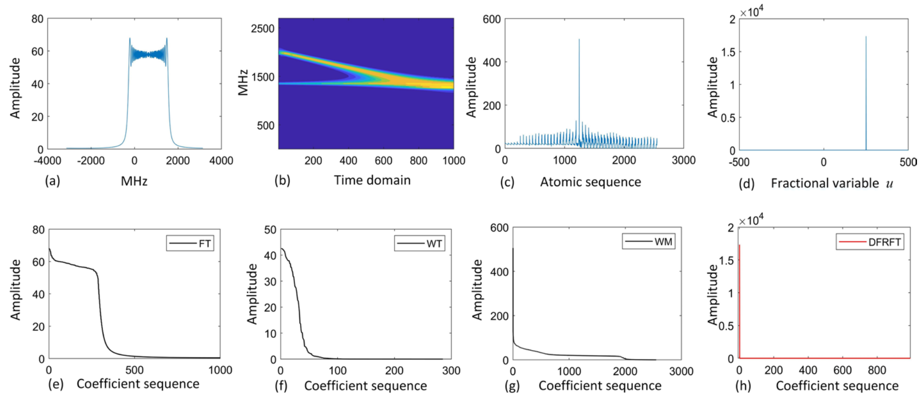

Fig. 5 Sparse representation of signal 1. **a** Sparse representation, FT; **b** sparse representation, WT; **c** sparse representation, WM; **d** sparse representation, DFRFT; **e** sparsity coefficient, FT; **f** sparsity coefficient, WT; **g** sparsity coefficient, WM; **h** sparsity coefficient, DFRFT

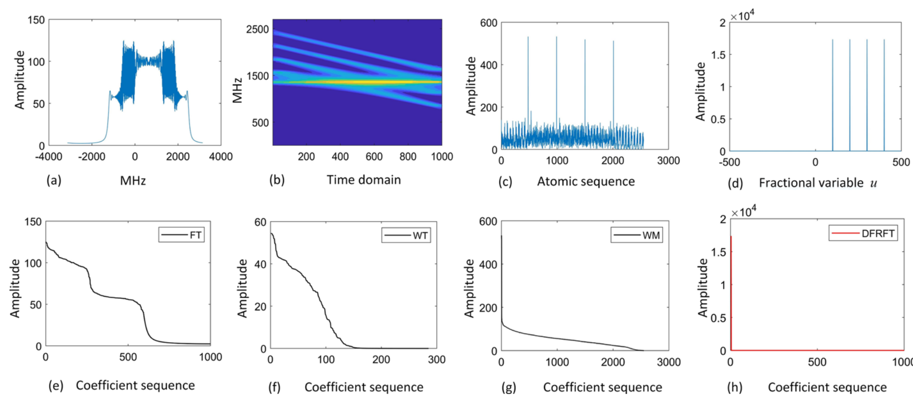

Fig. 6 Sparse representation of signal 2. **a** Sparse representation, FT; **b** sparse representation, WT; **c** sparse representation, WM; **d** sparse representation, DFRFT; **e** sparsity coefficient, FT; **f** sparsity coefficient, WT; **g** sparsity coefficient, WM; **h** sparsity coefficient, DFRFT

coefficients in descending order of amplitude is improved, but the compressibility is still limited. The sparse representation effect of method (3) is significantly improved, and the attenuation speed of the coefficient amplitude is obviously accelerated but still inferior to method (4). In summary, the sparse representation effect of signals under different dictionaries can be ranked as follows: Method (4) > Method (3) > Method (2) > Method (1); From the perspective of coefficient decay speed, the rapid decline of the sparse representation coefficient of the DFRFT dictionary is obviously faster than that of other dictionary methods, and the sparse representation effect and compressibility of the signal are better when the DFRFT dictionary is used.

3.3 Anti-noise analysis

Gaussian white noise is added to the simulation signal to replicate the complex battlefield environment and test the DFRFT dictionary's anti-noise performance. Because methods (1) and (2) have poor sparse representation effects, only methods (3) and (4)

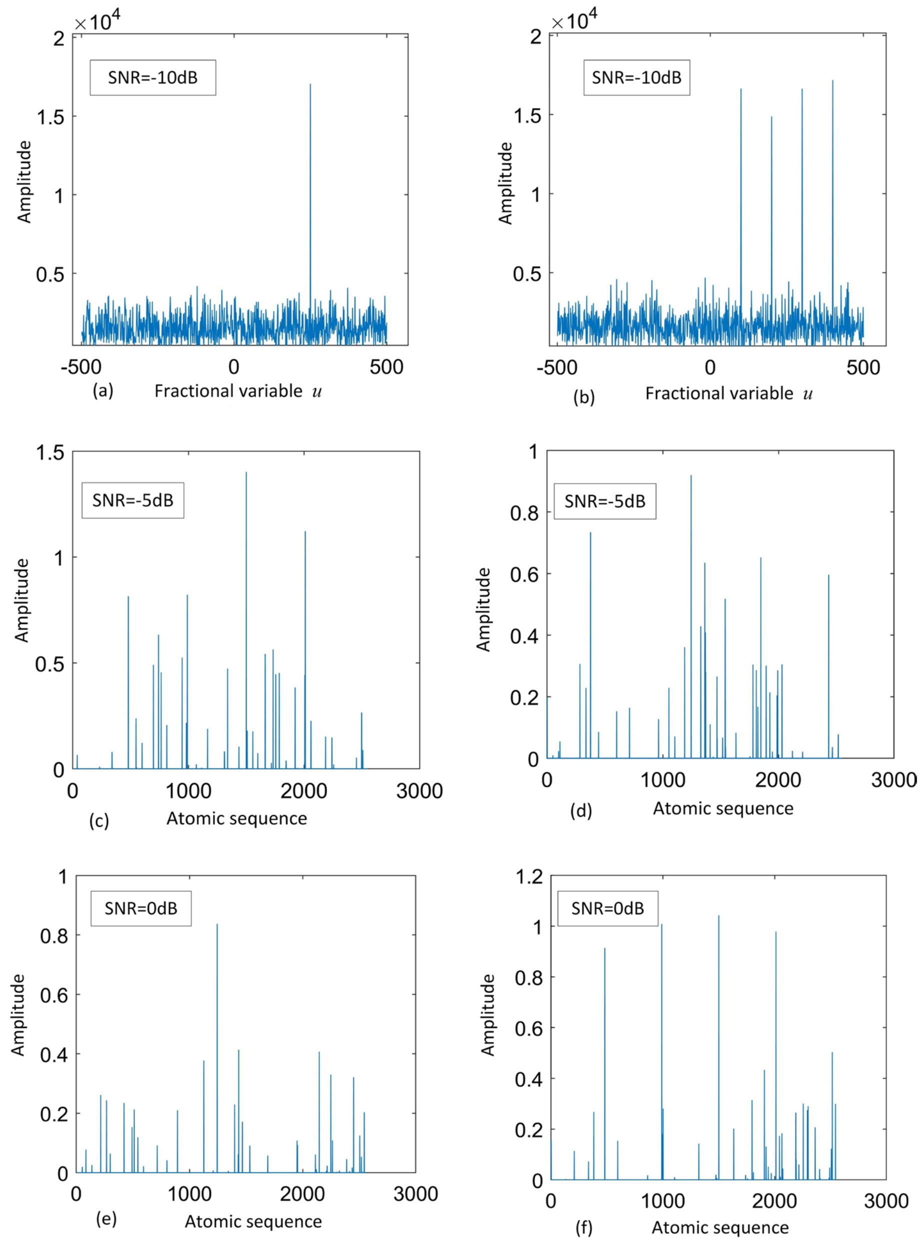

Fig. 7 Anti-noise performance analysis. **a** DFRFT with − 10 dB, $K=1$; **b** DFRFT with − 10 dB, $K=4$; **c** MW with − 5 dB, $K=1$; **d** MW with − 5 dB, $K=4$; **e** MW with 0 dB, $K=1$; **f** MW with 0 dB, $K=1$

are compared for their anti-noise performances. Because the proposed method (4) is noise immune, only the case of a − 10 dB condition is examined. Method (3) analyzes the cases of − 5 dB and 0 dB, respectively, and the results are shown in Fig. 7.

Figure 7a and b shows that, despite having the signal-to-noise ratio (SNR) of − 10 dB, the DFRFT dictionary still has good sparse representation results, indicating its strong anti-noise ability. The MW dictionary results in Fig. 7c–f. When SNR is − 5 dB, the sparse representation coefficients of signals in Fig. 7c and d are severely interfered with by noise and cannot be used to estimate signal parameters. When SNR is 0 dB, the atomic sequence corresponding to the signal sparse representation coefficient can still be seen. In general, the anti-noise performance of the DFRFT dictionary is obviously better than that of the WM dictionary.

3.4 Restricted isometry property (RIP) analysis

According to the literature [34], the compressed observation performance of the observation matrix or perception matrix may be assessed using the RIP characteristics, and the better the compressed observation performance, the higher the reconstruction accuracy of the recovered signal. For any signal $\boldsymbol{x}$ with sparsity k, if there is a minimum constant $\delta_k \in (0,1)$ such that the matrix $\boldsymbol{D}$ satisfies Eq. (20). Then, the matrix $\boldsymbol{D}$ is satisfied with RIP.

$$(1-\delta_k)\|\mathbf{x}\|_2^2 \leq \|\mathbf{Dx}\| \leq (1+\delta_k)\|\mathbf{x}\|_2^2 \tag{20}$$

where δ_k denotes the Restricted Isometry Constraints (RIC).

The RIP of the measurement matrix $\mathbf{\Phi}$ in this paper has been proven in Ref [18], and for the perceptual matrix $\boldsymbol{A}$, the smaller the correlation between the measurement matrix and the sparse dictionary, the better the compressed observation performance. The compressive observation performance of the perceptual matrix is assessed using the correlation coefficients between its column vectors. The maximum correlation coefficient is calculated as:

$$\mu_{\max}(\boldsymbol{A}) = \max_{1\leqslant i,j\leqslant n, i\neq j}\left(a_i^T a_j\right) \tag{21}$$

The average correlation coefficient is calculated as:

$$\mu_{av} = \frac{1}{n(n-1)}\sum_{1\leqslant i,j\leqslant k, i\neq j}^{n}(a_i^T a_j) \tag{22}$$

where a_i is the column vector of $\boldsymbol{A}$, n is the number of columns of $\boldsymbol{A}$.

For the four different sparse dictionaries used in this paper, the results of the representation of the correlation coefficients of their corresponding perceptual matrices are shown in Table 2. The results in Table 2 show that the proposed method has the smallest correlation coefficient compared to other methods. $\boldsymbol{A}_1$, $\boldsymbol{A}_2$, $\boldsymbol{A}_3$, $\boldsymbol{A}_4$ are the perceptual matrices obtained by multiplying four different dictionaries with the measurement matrix, respectively.

Table 2 Correlation coefficients of different methods

Perception matrix	$\mu_{\max}$	μ_{av}
$\boldsymbol{A}_1$ (Method 1)	0.2620	0.1720
$\boldsymbol{A}_2$ (Method 2)	0.2471	0.0622
$\boldsymbol{A}_3$ (Method 3)	0.2456	0.0319
$\boldsymbol{A}_4$ (Method 4)	**0.2351**	**0.0231**

Bold values indicate the best performance among the different methods

3.5 Algorithm complexity

Assuming N samples of the LFM signal, the total number of complex multiplications of the method (1) is approximately $O(N^2)$, and the computational complexity of the method (2) is approximately $O(N\log(N))$. The computational complexity of our proposed method is $O(2N^2)$, according to Eq. (14). When considering the WM dictionary construction process, the complexity of method (3) is irrelevant to the signal dimension but related to the division accuracy of the signal interval. Assuming that the signal frequency interval is divided into L parts and the computational complexity of the method (3) is $O(L^2)$, Table 3 displays the algorithm complexity.

According to Table 3, the complexity of the proposed method is on par with that of other methods, but it performs significantly better than other methods in terms of the sparse representation effect, noise immunity, and compressed observation performance.

Figure 8 presents a comparison of the construction time for different dictionaries under various signal dimensions. From the graph, it can be observed that the construction time of the FT dictionary and DFRFT dictionary increases linearly with the signal dimension. Additionally, the construction time of the DFRFT dictionary is approximately twice that of the FT dictionary. On the other hand, the WT dictionary exhibits a gradually stabilizing construction time as the signal dimension increases, highlighting its advantage for high-dimensional signals. However, it is evident that the WT dictionary is not the optimal strategy for low-dimensional signals obtained through compressed sampling. In contrast, the construction time of the WM dictionary is unrelated to the signal dimension, as it is determined by the construction method of the WM dictionary. The more intervals used in the dictionary construction process, the longer the construction time. Nevertheless, in most cases, the number of intervals in the WM dictionary is less than the signal dimension. Therefore, in

Table 3 Algorithm complexity

Algorithm	Complexity
Method (1)	$O(N^2)$
Method (2)	$O(N\log(N))$
Method (3)	$O(L^2)$
Method (4)	$O(2N^2)$

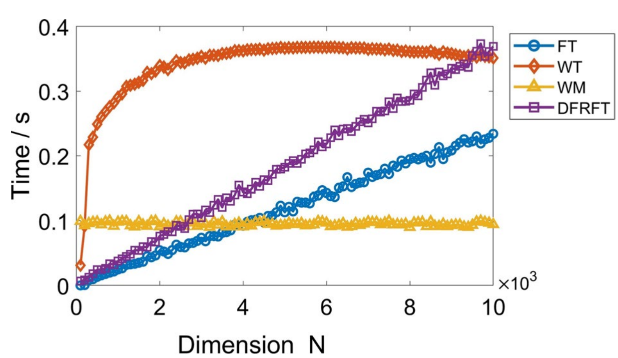

Fig. 8 Comparison of time consumption

terms of construction time, the waveform matching dictionary demonstrates higher construction efficiency. Consequently, when facing the parameter estimation problem of linear frequency modulation signals under known prior information, the waveform matching dictionary proves to be more time-efficient than the DFRFT dictionary.

4 Parameter estimation based on RD system

It is required to first ascertain the value of R for various LFM signals and then use the reconstruction error as the criterion to assess the validity of compressed sampling data because varied sampling rates (R) will have an impact on the compression sampling effect of RD systems. Signal reconstruction is deemed successful and the R value is valid when $E \leq 0.1$. The following is the definition of the reconstruction error equation:

$$E = \frac{\left\|\widehat{x}(t) - x(t)\right\|_2}{\|x(t)\|_2} \tag{23}$$

where $\widehat{x}(t)$ is reconstructed signal, $\|\cdot\|_2$ is $L2$ norm.

The recovery algorithm is used to recover the compressed sampling data with different R values, and the relationship between R and signal reconstruction success probability is shown in Fig. 8.

Figure 9 shows that for $R = 40$, the signal reconstruction effect is guaranteed, showing that the compressed sampling data is effective. The simulation signal is sampled using the RD compression sampling technique, and the compression sampling is presented in Table 4. Table 4 shows that the RD system can perform signal compression sampling with a lower sample frequency and sampling locations.

After obtaining the compressed sampling data, create DFRFT dictionaries of different orders by dividing the order p equally in the interval [0, 2) in steps of 0.01, creating 200 DFRFT dictionaries corresponding to different orders p, and then recovering the compressed sampling data in conjunction with the reconstruction algorithm to obtain the sparse representation coefficients corresponding to different DFRFT dictionaries. Figure 10 depicts the two-dimensional distribution.

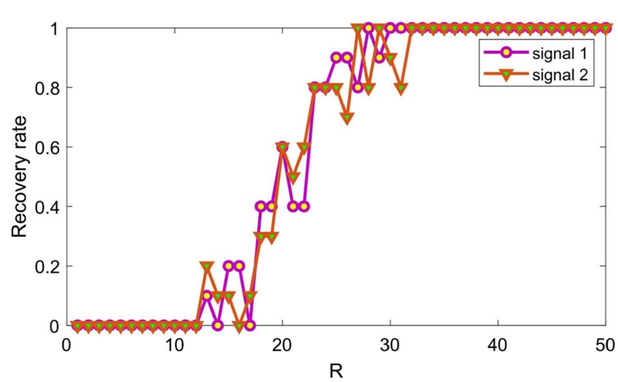

Fig. 9 Reconstruction probability

Table 4 Compressed sampling of RD system

Signal	Sampling method	Sampling frequency (MHz)	Sampling points	Compression ratio
Signal 1	Nyquist	1000	1000	–
	RD	**40**	**40**	**15: 1**
Signal 2	Nyquist	1000	1000	–
	RD	**40**	**40**	**15: 1**

Bold values indicate the best performance among the different methods

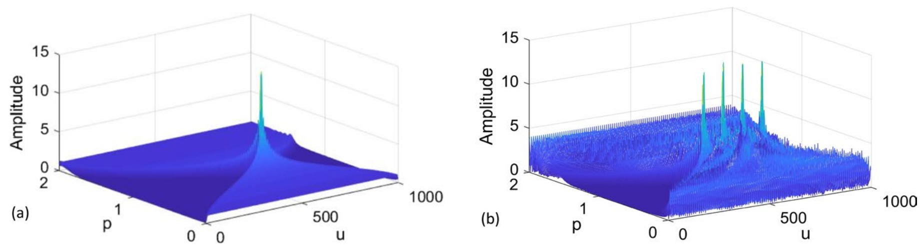

Fig. 10 The $|\mathbf{r}_{\mathrm{FR}}(p,u)|$ of simulation signal. **a** Signal 1; **b** Signal 2

Search the peak position of $|\mathbf{r}_{\mathrm{FR}}(p,u)|$ in the graph to get $(\widehat{p}_{\mathrm{opt}},\ \widehat{u}_{\mathrm{opt}})$.We compare the QPSO algorithm with the GA-PSO algorithm, the PSO algorithm, the 2-DS algorithm, and the swarm optimization (PSO) algorithm. In the experiment, the starting population size of PSO, GA-PSO, and QPSO is set to 50, the maximum number of iterations is 30, and the particle swarm position is initialized at random on the $(p,\ u)$ plane. The step size of the two-dimensional search technique is also set to 0.01. Equation (19) represents the fitness function, and Fig. 11 depicts the algorithm's convergence phase. Tables 5 and 6 respectively display the parameter estimation results for single-component and multi-component signals.

From the convergence process in Fig. 11, it is obvious that the QPSO algorithm is superior to other algorithms in terms of convergence speed and convergence accuracy. After the PSO algorithm converges to a certain extent, the convergence accuracy cannot be improved, and it is trapped in a local optimal solution and cannot further converge. Compared with PSO algorithm, GA-PSO algorithm has improved in convergence speed and convergence precision, but its complexity is higher than QPSO algorithm, which affects the convergence speed.

In Tables 5 and 6, although the direct search algorithm ensures the search accuracy within the step size range, its operation time is much longer than that of other algorithms. The calculation efficiency of the PSO algorithm has been greatly improved, but the existence of local optimization problems has affected the accuracy of parameter estimation. The GA-PSO algorithm has been improved, but the increase in algorithm complexity leads to its operation taking longer than the QPSO algorithm.

To validate the effectiveness of the proposed method in this paper, a comparative experimental analysis was conducted using the simulated signals generated in this section. Three different comparative methods were employed during the experimental process:

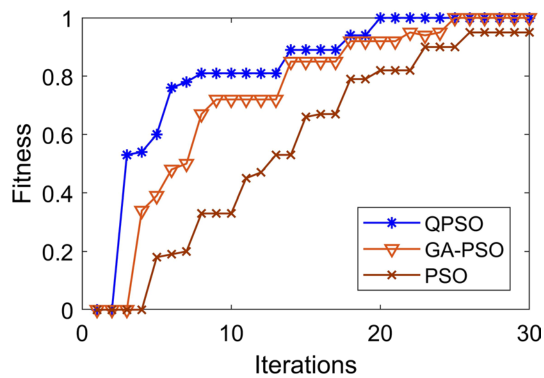

Fig. 11 Iterative process

Table 5 Estimated parameters of signal

Methods	$(\widehat{p}_{\text{opt}}, \widehat{u}_{\text{opt}})$	$(\widehat{k}, \widehat{f_c})$	Error $(\widehat{k})$	Error $(\widehat{f_c})$	Operation time/s
QPSO	**(0.81, 595)**	**(307.8, 255.3)**	**0.026**	**0.021**	**10.23**
GA-PSO	(0.81, 595)	(307.8, 255.3)	0.026	0.021	20.33
PSO	(0.79, 590)	(323.9, 264.7)	0.080	0.059	50.76
2-DS	(0.81, 595)	(307.8, 255.3)	0.026	0.021	264

Bold values indicate the best performance among the different methods

Table 6 Estimated parameters of signal 2

Methods	$(\widehat{p}_{\text{opt}}, \widehat{u}_{\text{opt}})$	$(\widehat{k}, \widehat{f_c})$	Error $(\widehat{k})$	Error $(\widehat{f_c})$	Operation time/s
QPSO	**(0.81, 454)**	**(− 307.8, 102.9)**	**0.026**	**0.029**	**12.23**
	(0.81, 549)	**(− 307.8, 204.5)**		**0.025**	
	(0.81, 645)	**(− 307.8, 305.1)**		**0.017**	
	(0.81, 738)	**(− 307.8, 407.7)**		**0.019**	
GA-PSO	(0.81, 454)	(− 307.8, 102.9)	0.026	0.029	24.33
	(0.81, 549)	(− 307.8, 204.5)		0.025	
	(0.81, 645)	(− 307.8, 305.1)		0.017	
	(0.81, 738)	(− 307.8, 407.7)		0.019	
PSO	(0.79, 443)	(− 323.9,109.3)	0.080	0.093	74.33
	(0.79, 545)	(− 323.9, 217.5)		0.088	
	(0.79, 641)	(− 323.9, 329.2)		0.097	
	(0.79, 729)	(− 323.9, 438.5)		0.096	
2-DS	(0.81, 454)	(− 307.8, 102.9)	0.026	0.029	684
	(0.81, 549)	(− 307.8, 204.5)		0.025	
	(0.81, 645)	(− 307.8, 305.1)		0.017	
	(0.81, 738)	(− 307.8, 407.7)		0.019	

Bold values indicate the best performance among the different methods

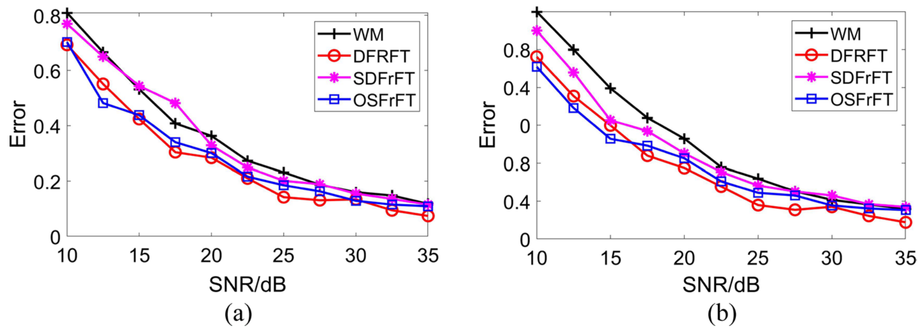

Fig. 12 Parameter estimation errors of the four methods under different SNR. **a** Parameter estimation error of frequency slope. **b** Parameter estimation error of initial frequency

(1) The method proposed in this paper: DFRFT.
(2) Waveform matching dictionary: MW [35].
(3) Sparse discrete fractional Fourier transform: SDFrFT [36].
(4) Optimized sparse fractional Fourier transform: OSFrFT [37].

The latter three methods were derived from the latest research achievements as documented in Refs [35–38]. They are considered cutting-edge in the field. The relative average error was adopted as the evaluation metric, and the parameter estimation errors of the four methods under different SNR conditions are depicted in Fig. 12. As shown in Fig. 12, as the SNR increases, the error in parameter estimation gradually decreases and reaches a plateau. However, in terms of the final parameter estimation results, the method proposed in this paper exhibits higher accuracy. However, in terms of efficiency in the actual operation process, SDFrFT and OSFrFT greatly simplify the complexity of dictionary construction, thus having higher computational efficiency.

5 Measured signal analysis

As seen in Fig. 13, the experiment uses the M9381A vector signal generator and the M9391A vector signal analyzer to create and gather LFM signals. The gathered data is then examined using Matlab R2018b.

Two single-component LFM signals were generated and collected in the experiment. Table 7 shows the signal parameter settings, and Fig. 14 shows the measured signal time domain waveform. First, the value of the RD system's sampling rate R is discussed, and Fig. 15 depicts the relationship between the reconstruction error and R. Using the results of Fig. 15, the compression sampling parameters are set as shown in Table 8, and the RD compression sampling system is used to compress and sample the measured signal. The compressed sampling data is then recovered using the DFRFT dictionary and OMP algorithm to obtain the sparse representation coefficients $\mathbf{r}(p,u)$ of the measured signal. And Fig. 16 displays the $|\mathbf{r}(p,u)|$ distribution of signals 3 and 4.

In Table 8, compared with traditional Nyquist sampling, the RD system can complete the compression sampling of the measured signal with a higher compression rate, a lower sampling frequency, and fewer sampling points. It can be seen from Fig. 15 that the method proposed in this manuscript has a good sparse representation effect for the measured signal, and the parameter estimation result with a low error can be obtained by combining the QPSO algorithm.

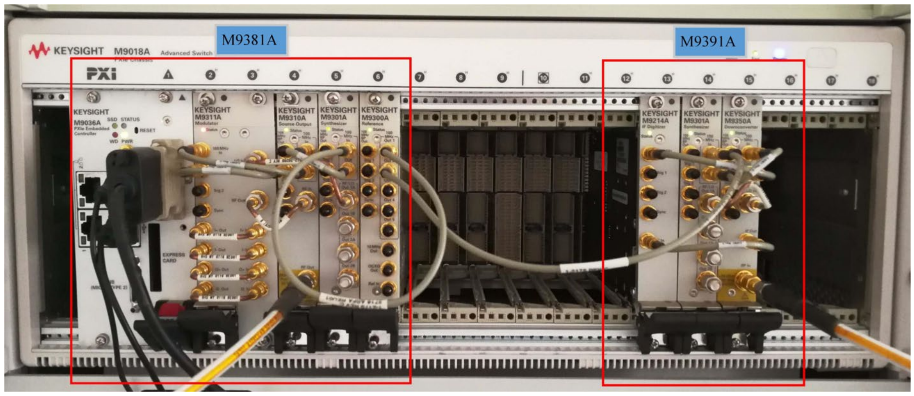

Fig. 13 M9381A vector signal generator and M9391A vector signal analyzer

Table 7 Parameters of measured signal

Signal	*K*	A_i (10^{-3})	f_i (GHz)	*B* (MHz)	*T* (us)
Signal 3	1	2	1.3	100	20.41
Signal 4	2	1	[0.8 1.2]	120	17.08

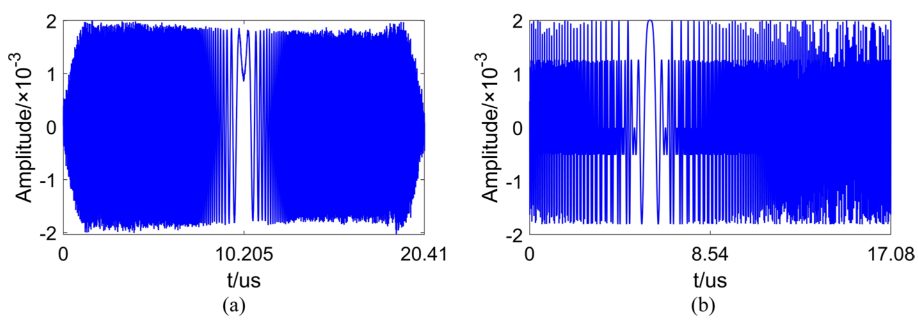

Fig. 14 Measured signal. **a** Signal 3; **b** Signal 4

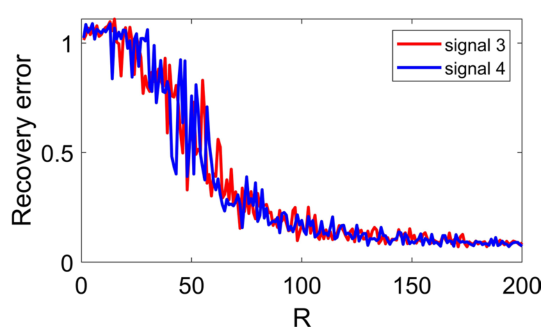

Fig. 15 The recovery error of measured signals with different *R*

By employing different parameter estimation methods from Sect. 4 to analyze the measured signals, the parameter estimation errors of each method are presented in Table 9.

Table 8 Comparison for sampling and analysis

Signal	Sampling method	Sampling frequency (MHz)	Sampling points	Compression ratio
Signal 3	Nyquist	150	3061	–
	RD	**8**	**163**	**18.75:1**
Signal 4	Nyquist	150	2562	–
	RD	**10**	**171**	**15: 1**

Bold values indicate the best performance among the different methods

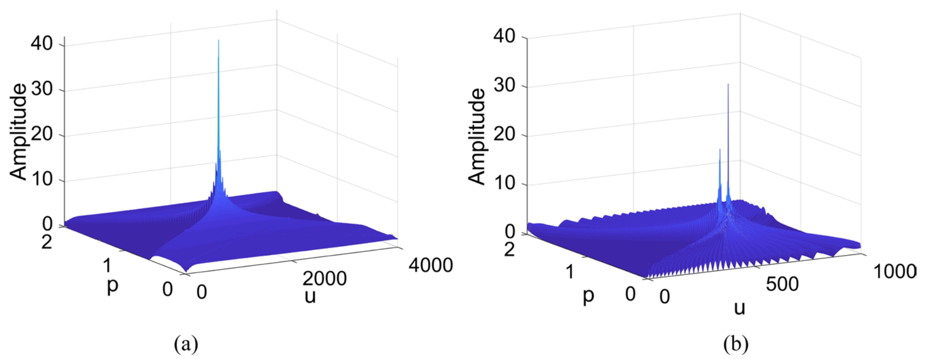

Fig. 16 The $|\mathbf{r}(p, u)|$ of measured signal. **a** Signal 3; **b** Signal 4

Table 9 Analysis of measured signals using various parameter estimation algorithms

Signal	Algorithm	Error: $k_e = \sum_{i=1}^{K} k_{i,e}$	Error: $f_e = \sum_{i=1}^{K} f_{i,e}$	Time/s
Signal 3	RD + DFRFT	**0.029**	**0.024**	10.51
	RD + SDFrFT	0.031	0.033	8.33
	RD + OSFrFT	0.034	0.027	**6.97**
	RD + WM	0.045	0.051	9.39
Signal 4	RD + DFRFT	**0.059**	**0.053**	12.65
	RD + SDFrFT	0.059	0.057	10.44
	RD + OSFrFT	0.063	0.054	**9.31**
	RD + WM	0.087	0.099	12.22

Bold values indicate the best performance among the different methods

According to the results presented in Table 9, it can be observed that the parameter estimation accuracies of the DFRFT, SDFrFT, and OSFrFT methods are remarkably close. However, the proposed method in this paper still exhibits the highest level of parameter estimation accuracy. Additionally, both the SDFrFT and OSFrFT methods demonstrate shorter dictionary construction time, with the OSFrFT dictionary construction being the fastest. This might be attributed to the fact that while the SDFrFT and OSFrFT methods reduce the complexity of dictionary construction, they slightly compromise the accuracy of parameter estimation.

To further elucidate the efficacy of LFM signals parameter estimation, this study incorporates a comparative analysis of recovery errors. By employing the estimated parameter information and Eq. (3), which governs LFM signals, the restoration of LFM signals is accomplished. The reconstructed LFM signals are subsequently juxtaposed with the

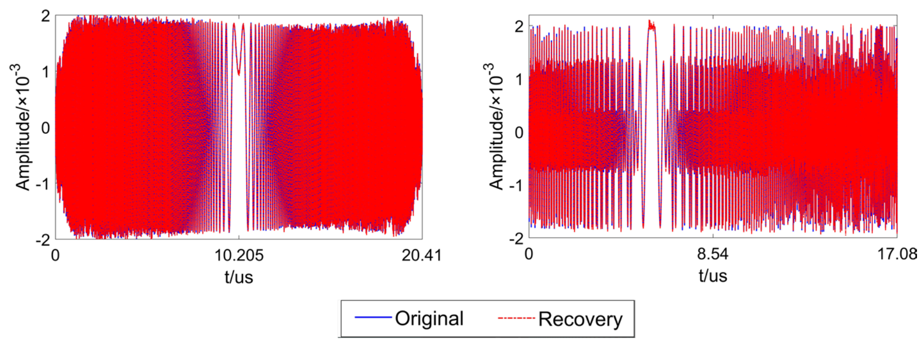

Fig. 17 Recovery error analysis

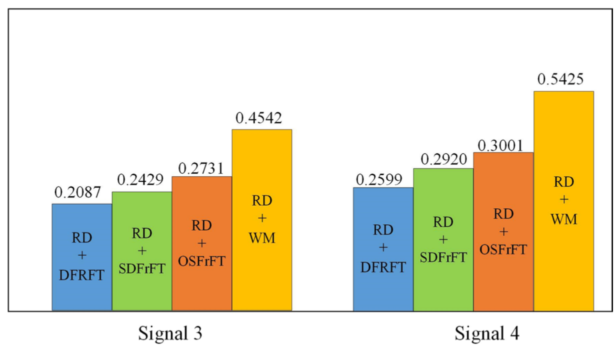

Fig. 18 The recovery errors of different methods

original ones, as depicted in Fig. 17, showcasing the outcomes of the proposed method. Observing the results shown in Fig. 17, it can be seen that the proposed method has basically achieved signal reconstruction.

Conducted comparative experiments with different methods. The reconstruction errors for Signal 3 and Signal 4, obtained using the four aforementioned methods, are depicted in Fig. 18. It can be observed from the figure that the proposed method in this paper exhibits the highest level of reconstruction accuracy. The reconstruction accuracy of the MW dictionary method is the poorest, while the reconstruction accuracy of the SDFrFT and OSFrFT dictionary methods is comparable to that of the proposed method.

6 Conclusion

To solve the parameter estimation problem of the LFM signal without reconstructing the original LFM signal, a method combining RD compression sampling and DFRFT dictionary is proposed in this manuscript. The validity of the compressed sampling data is ensured during the compression sampling stage by determining the value of the sampling rate R. The compressed sampled data are then analyzed by constructing the DFRFT dictionary and combining it with the recovery algorithm and the parameter optimization algorithm, and the parameters of the original signal are estimated directly using the compressed sampled data. The correlation between compressed sampling data and signal parameters can be established based on the construction principle of the DFRFT dictionary, which provides a theoretical basis for directly estimating LFM signal parameters using compressed sampling data. The experimental results show that the proposed method has good sparse representation and anti-noise performance and can ensure good accuracy in parameter estimation of LFM signals.

However, compared to some improved SDFrFT and OSFrFT sparse dictionary construction methods, although the proposed method has high parameter estimation accuracy, there is still room for improvement in reducing dictionary complexity and improving operational efficiency.

Acknowledgements
The authors would like to sincerely thank all the anonymous reviewers for their valuable comments that greatly helped improve the manuscript.

Funding
National Natural Science Foundation of China (61501493).

Availability of data and materials
The data that support the findings of this study are available on request from the corresponding author. The data are not publicly available due to privacy or ethical restrictions.

Declarations

Competing interests
The authors declare no conflict of interest.

Received: 12 April 2023 Accepted: 15 September 2023
Published online: 23 September 2023

References

1. S.S. Moghadasian, A fast and accurate method for parameter estimation of multi-component LFM signals. IEEE Signal Process. Lett. **29**, 1719–1723 (2022)
2. Y. Xing et al., Design of a robust radio-frequency fingerprint identification scheme for multimode LFM radar. IEEE Internet Things J. **7**, 10581–10593 (2020)
3. R. Song et al., OFDM-NOMA combined with LFM signal for W-band communication and radar detection simultaneously. Opt. Lett. **47**, 2931–2934 (2022)
4. M. Mercuri, Y. Lu, S. Polito et al., Enabling robust radar-based localization and vital signs monitoring in multipath propagation environments. IEEE Trans. Biomed. Eng. **68**, 3228–3240 (2021)
5. W. Cheng, Q. Zhang, J. Dong et al., An enhanced algorithm for deinterleaving mixed radar signals. IEEE Trans. Aerosp. Electron. Syst. **57**, 3927–3940 (2021)
6. Y. Shen, H. Li, H. Xin et al., A 103-dB SFDR calibration-free oversampled SAR ADC with mismatch error shaping and pre-comparison techniques. IEEE J. Solid-State Circuits **57**, 734–744 (2021)
7. Z. Zhu et al., A 14-bit 4-MS/s VCO-based SAR ADC with deep metastability facilitated mismatch calibration. IEEE J. Solid-State Circuits **55**, 1565–1576 (2020)
8. J. Chen, J. Zhang, Y. Jin et al., Real-time processing of spaceborne SAR data with nonlinear trajectory based on variable PRF. IEEE Trans. Geosci. Remote Sens. **60**, 1–12 (2021)
9. E.J. Candès et al., Robust uncertainty principles: exact signal reconstruction from highly incomplete frequency information. IEEE Trans. Inf. Theory **52**, 489–509 (2006)
10. X. Lu, W. Su, J. Yang et al., Radio frequency interference suppression for SAR via block sparse Bayesian learning. IEEE J. Sel. Top. Appl. Earth Obs. Remote Sens. **11**, 4835–4847 (2018)
11. L. Zou, Z. Wang, D. Zhou, Moving horizon estimation with non-uniform sampling under component-based dynamic event-triggered transmission. Automatica **120**, 109154 (2020)
12. C. Qin, C.C. Chang, P.L. Tsou, Robust image hashing using non-uniform sampling in discrete Fourier domain. Digit. Signal Process. **23**, 578–585 (2013)
13. A. Mirigaldi, M. Carbone, G. Perrone, Non-uniform adaptive angular spectrum method and its application to neural network assisted coherent beam combining. Opt. Express **29**, 13269–13287 (2021)
14. H. Zhao et al., Generalized random demodulator associated with fractional Fourier transform. Circuits Syst. Signal Process. **37**, 5161–5173 (2018)
15. S. Jiang, N. Fu, L. Qiao, et al., Joint carrier and 2D-DOA estimation for MWC based on two L-shaped arrays, in *International Instrumentation and Measurement Technology Conference*. IEEE (2019)
16. G. Iadarola, P. Daponte, L. De Vito et al., On the effects of PRBS non-idealities in signal reconstruction from AICs. IEEE Trans. Instrum. Meas. **72**, 1–11 (2023)
17. M.A. Davenport, J.N. Laska, J.R. Treichler et al., The pros and cons of compressive sensing for wideband signal acquisition: noise folding versus dynamic range. IEEE Trans. Signal Process. **60**, 4628–4642 (2012)
18. J.A. Tropp et al., Beyond Nyquist: efficient sampling of sparse bandlimited signals. IEEE Trans. Inf. Theory **56**, 520–543 (2010)
19. Y. Guo et al., Parameter estimation of frequency hopping signal based on MWC–MSBL reconstruction. IET Commun. **14**, 1642–1649 (2020)

20. T. Chen, L. Liu, X. Huang, LPI radar waveform recognition based on multi-branch MWC compressed sampling receiver. IEEE Access **6**, 30342–30354 (2018)
21. G. Iadarola, IMS awards: characterization of analog-to-information converters. IEEE Instrum. Meas. Mag. **25**, 98–99 (2022)
22. O. Taheri et al., Segmented compressed sampling for analog-to-information conversion: method and performance analysis. IEEE Trans. Signal Process. **59**, 554–572 (2011)
23. D. Healy, Analog-to-information [R] Arlington: Defense Advanced Research Projects Agency (2005)
24. M.A. Davenport et al., Signal processing with compressive measurements. IEEE J. Sel. Top. Signal Process. **4**, 445–460 (2010)
25. Y. Wang, N. Cao, Y. Cui et al., Real time dynamic magnetic resonance imaging via dictionary learning and combined Fourier transform. IEEE Access. **7**, 150924–150935 (2019)
26. B.S. Shaik, V.K. Chakka, A.S. Reddy, A new signal representation using complex conjugate pair sums. IEEE Signal Process. Lett. **26**, 252–256 (2019)
27. M. Yu, Z. Tang, X. Zhang et al., Perceptual hashing with complementary color wavelet transform and compressed sensing for reduced-reference image quality assessment. IEEE Trans. Circuits Syst. Video Technol. **32**, 7559–7574 (2022)
28. Z. Lin, S. Jia, X. Zhou et al., Digital holographic microscopy phase noise reduction based on an over-complete chunked discrete cosine transform sparse dictionary. Opt. Lasers Eng. **166**, 107571 (2023)
29. F. Deng, Y. Qiang, S. Yang et al., Sparse representation of parametric dictionary based on fault impact matching for wheelset bearing fault diagnosis. ISA Trans. **110**, 368–378 (2021)
30. J. Peng, W. Sun, H.C. Li et al., Low-rank and sparse representation for hyperspectral image processing: a review. IEEE Geosci. Remote Sens. Mag. **10**, 10–43 (2021)
31. C. Pang, S. Liu, Y. Han, High-Speed target detection algorithm based on sparse Fourier transform. IEEE Access **6**, 37828–37836 (2018)
32. S.C. Pei et al., Closed-form discrete fractional and affine Fourier transforms. IEEE Trans. Signal Process. **48**, 1338–1353 (2000)
33. T.M. Shami, A.A. El-Saleh, M. Alswaitti et al., Particle swarm optimization: a comprehensive survey. IEEE Access **10**, 10031–10061 (2022)
34. Y. Ding, D. Kunisky, A.S. Wein et al., The average-case time complexity of certifying the restricted isometry property. IEEE Trans. Inf. Theory **67**, 7355–7361 (2021)
35. S. Meng, C. Meng, C. Wang, Method based on random demodulator and waveform matching dictionary to estimate LFM signal parameter. J. Sens. **2023**, 1–11 (2023)
36. S. Liu, T. Shan, R. Tao et al., Sparse discrete fractional Fourier transform and its applications. IEEE Trans. Signal Process. **62**, 6582–6595 (2014)
37. H. Zhang, T. Shan, S. Liu et al., Optimized sparse fractional Fourier transform: principle and performance analysis. Signal Process. **174**, 107646 (2020)
38. C. Pang, S. Liu, Y. Han, Coherent detection algorithm for radar maneuvering targets based on discrete polynomial-phase transform. IEEE J. Sel. Top. Appl. Earth Obs. Remote Sens. **12**, 3412–3422 (2019)

Publisher's Note